

Non-linear IV characteristics in two-dimensional superconductors: Berezinskii-Kosterlitz-Thouless physics vs inhomogeneity

G. Venditti,¹ J. Biscaras,² S. Hurand,^{3,4} N. Bergeal,^{3,5} J. Lesueur,^{3,5} A. Dogra,⁶ R. C. Budhani,⁷
Mintu Mondal,^{8,9} John Jesudasan,⁹ Pratap Raychaudhuri,⁹ S. Caprara,¹ and L. Benfatto^{1,*}

¹*ISC-CNR and Dep. of Physics, Sapienza University of Rome, P.le A. Moro 5, 00185 Rome, Italy*

²*Sorbonne Université, CNRS, MNHN, Institut de Minéralogie de Physique
des Matériaux et de Cosmochimie, IMPMC, F-75005 Paris, France*

³*Laboratoire de Physique et d'Etude des Matériaux, ESPCI Paris,
PSL Research University, CNRS, 10 Rue Vauquelin - 75005 Paris, France*

⁴*Institute Pprime, UPR 3346 CNRS, Université de Poitiers,
ISAE-ENSMA, BP 30179, 86962 Futuroscope-Chasseneuil Cedex, France*

⁵*Université Pierre and Marie Curie, Sorbonne-Universités, 75005 Paris, France*

⁶*National Physical Laboratory, New Delhi, 110012, India*

⁷*Department of Physics, Morgan State University, Baltimore, Maryland 21251, USA*

⁸*School of Physical Sciences, Indian Association for the Cultivation of Science, Jadavpur, Kolkata 700032, India*

⁹*Tata Institute of Fundamental Research, Homi Bhabha Rd, Colaba, Mumbai 400005, India*

(Dated: September 1, 2022)

One of the hallmarks of the Berezinskii-Kosterlitz-Thouless (BKT) transition in two-dimensional (2D) superconductors is the universal jump of the superfluid density, that can be indirectly probed via the non-linear exponent of the current-voltage IV characteristics. Here, we compare the experimental measurements of IV characteristics in two cases, namely NbN thin films and SrTiO₃-based interfaces. While the former display a paradigmatic example of BKT-like non-linear effects, the latter do not seem to justify a BKT analysis. Rather, the observed IV characteristics can be well reproduced theoretically by modelling the effect of mesoscopic inhomogeneity of the superconducting state. Our results offer an alternative perspective on the spontaneous fragmentation of the superconducting background in confined 2D systems.

The progress in material science has made nowadays available a wide class of systems with thickness ranging from a few nanometers down to the atomic-layer limit. The possibility to engineer these effectively two-dimensional (2D) materials in field-effect devices opens also the exciting possibility to tune their quantum-mechanical ground state by changing the electron density. In some remarkable cases, including transition-metal dichalcogenides[1], SrTiO₃-based oxide interfaces[2], such as LaAlO₃/SrTiO₃ and LaTiO₃/SrTiO₃ (LTO/STO), and the recently discovered twisted graphene[3], the ground state can be continuously tuned from metallic/insulating to superconducting (SC). How the reduced dimensionality influences both phases is still a largely open question, which challenges our basic understanding of the collective fluctuations in 2D systems.

A particularly interesting issue about 2D SC materials regards the very nature of the SC transition, that is expected to be described by the Berezinskii-Kosterlitz-Thouless (BKT) theory [4–6]. This expectation is based on symmetry arguments, since the SC transition in these systems belongs to the same universality class of the 2D XY model, that can be viewed as an effective coarse-grained model for phase of the SC order parameter, especially when the system is thin enough to avoid the screening effects of charged supercurrents [7]. The relevant excitations in this case are topological vortex-like configurations of the phase, and the energy scale is set by the superfluid stiffness $J_s = \hbar^2 n_s / 4m = \hbar^2 c^2 d / 16\pi e^2 \lambda^2$,

where n_s is the 2D superfluid density, λ the penetration depth, and d the film thickness. Within the BKT scenario, the transition to the normal state is driven by the thermal unbinding of vortex-antivortex pairs, that leads to specific signatures, the most striking being the discontinuous jump [8] of J_s from a finite value right below T_{BKT} to zero above it, with an universal ratio $J_s(T_{BKT}^-) / T_{BKT} = 2/\pi$. This feature is in principle observable via direct measurements of $\lambda(T)$, or it can be inferred from the measurements of the non-linear exponent of the IV characteristics [9], that is ruled by the breaking of vortex-antivortex pairs induced by a large enough current.

In practice, the experimental observation of the BKT transition in real systems is far from being straightforward. The most crucial limitation comes from the fact that in clean thick films J_s is much larger than the critical temperature, so that the temperature T_{BKT} where $J_s(T_{BKT}) \simeq T_{BKT}$ is indistinguishable from the T_c at which pairing disappears. In few-nanometer thick films of conventional superconductors, like NbN or MoGe, the BKT scale becomes accessible, thanks to the fact that in such ultrathin films n_s (and then J_s) is strongly suppressed by disorder [1, 2, 10–15, 18–20]. A similar condition can be reached in STO-based interfaces, where an extremely fragile SC condensate was recently reported [21–23]. However, in both cases the increase of disorder comes along with an increasing *inhomogeneity* of the SC background, on length scales that can be different in dif-

ferent systems, questioning the very applicability of the standard theoretical expectations based on the *clean XY* model [1, 24–31]. In the case of thin films of conventional superconductors the SC backgrounds fragments into islands with typical size of tens of nanometers [32–38]. As a consequence, the superfluid-density jump is smeared but is still observable either via the direct measurement of the inverse penetration depth [1, 2, 13–15, 18–20], or via the measurement of the exponent of the non-linear *IV* characteristics near T_c [10–12]. On the other hand, for STO-based interfaces there has been increasing evidence that the SC background organizes in islands of larger size [8, 39–42], so that the broadening of the resistive transition itself has been ascribed to a percolation mechanism via a network of SC puddles [7, 25, 45]. For what concerns the BKT physics, the direct measurement of the J_s is rather challenging, and few experimental reports exist so far [22, 23]. As a consequence, the occurrence or not of a BKT-like transition has been usually inferred from the analysis of the *IV* characteristics [40, 46–48]. However, despite the common assignment in support of a BKT scenario, the behavior of the stiffness extracted by the non-linear transport is far from being the one expected in the BKT case, as we shall discuss further below.

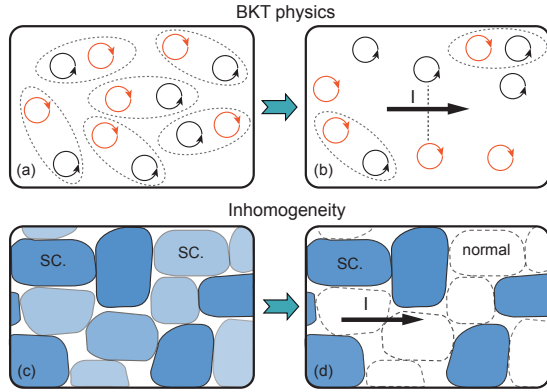


Figure 1. Generation of non-linear *IV* characteristics due to BKT physics (upper panels) and inhomogeneity (lower panels). In the BKT case the vortices, which are bound below T_c in pairs with opposite vorticity (panel a), get unbound by a sufficiently large current I (panel b). This generates an extra voltage drop proportional to the average density of unbound vortices, leading to non-linear characteristics. In the case of inhomogeneous superconductors instead the system segregates into puddles with different strength of the local SC condensate (panel c). As a consequence, a finite applied current I can turn weak SC puddles into normal ones (panel d), non-linearly increasing the global resistivity.

In this Letter we analyze the role of SC inhomogeneity in the non-linear *IV* characteristics of 2D superconductors. We compare two paradigmatic systems: NbN thin films and STO-based interfaces. In the former case we show that the superfluid-stiffness behavior extracted from the measurements of the *IV* characteristics is con-

sistent with the direct measurements of λ^{-2} , and both are compatible with a BKT transition, even if the BKT universal jump is smeared by disorder [1, 19, 27, 30]. In contrast, for STO-based interfaces the non-linearity of the *IV* characteristics cannot be simply ascribed to vortex-antivortex unbinding triggered by a large current, as it happens within the BKT scheme, since this would lead to dramatically overestimate the BKT transition temperature. We then argue that in these systems the non-linearity of the *IV* characteristics is due to the pair-breaking effect in the weaker SC regions, as the driving current increases, see Fig. 1. By modelling this mechanism within an effective medium (EM) theory, we can reproduce a *IV* non-linearity in qualitative agreement with the experiments, suggesting that mesoscopic inhomogeneity can essentially hinder the observation of BKT effects at these interfaces.

Let us start with the case of a 3nm NbN thin film, whose *IV* characteristics are shown in Fig. 2a (see [49] for details of the measurements). As mentioned above, within the BKT scenario the *IV* characteristics acquire a non-linear dependence near T_c , since a large enough current can unbind the vortex-antivortex pairs present below T_c . This effect generates a voltage $V \propto n_V(I)I$, where the equilibrium density of free vortices $n_V(I)$ scales with a power-law of the applied current, with an exponent proportional to J_s [9]:

$$V \propto I^{a(T)}, \quad a(T) = 1 + \frac{\pi J_s(T)}{T}. \quad (1)$$

In the ideal BKT case [4, 6, 8] the discontinuous jump of $J_s(T)$ at the transition translates into the jump of the *IV* exponent from $a(T_{BKT}^-) = 3$ to $a = 1$. In real 2D superconductors, as NbN thin films, the J_s^λ obtained by direct measurements of λ^{-2} by means of two-coil mutual inductance technique [1–3] displays a rapid but smeared downturn, see Fig. 2b, that can be explained accounting for a moderate inhomogeneity of the sample, and for the small vortex-core energy [1, 19, 27]. As a consequence, the real BKT temperature is not at the intersection with the universal BKT line $2T/\pi$, but it is the scale T_c where $J_s^\lambda = 0$. In Fig. 2b we show that $J_s^a(T) \equiv (a - 1)T/\pi$, extracted from the *IV* exponent $a(T)$, closely matches $J_s^\lambda(T)$ below T_c , and vanishes at a slightly larger T . This phenomenon can be ascribed to finite-size effects, since the current used to estimate J_s^a from Eq. (1) sets a finite length scale which rounds off the vanishing of the stiffness above T_{BKT} [5]. This is the same effect usually seen while measuring the stiffness at finite microwave frequencies [14, 15, 20]. Thus, the critical temperature T_c^a identified by the vanishing of J_s^a , i.e., $a(T_c^a) = 1$, is only few percent larger than the true T_c set by dc transport, $R(T_c) = 0$, or by the vanishing of J_s^λ . We also notice that the temperature T_{BKT}^a where $a(T_{BKT}^a) = 3$ has no particular significance in the realistic case of a smeared jump, but it is still expected to be lower than the real T_c .

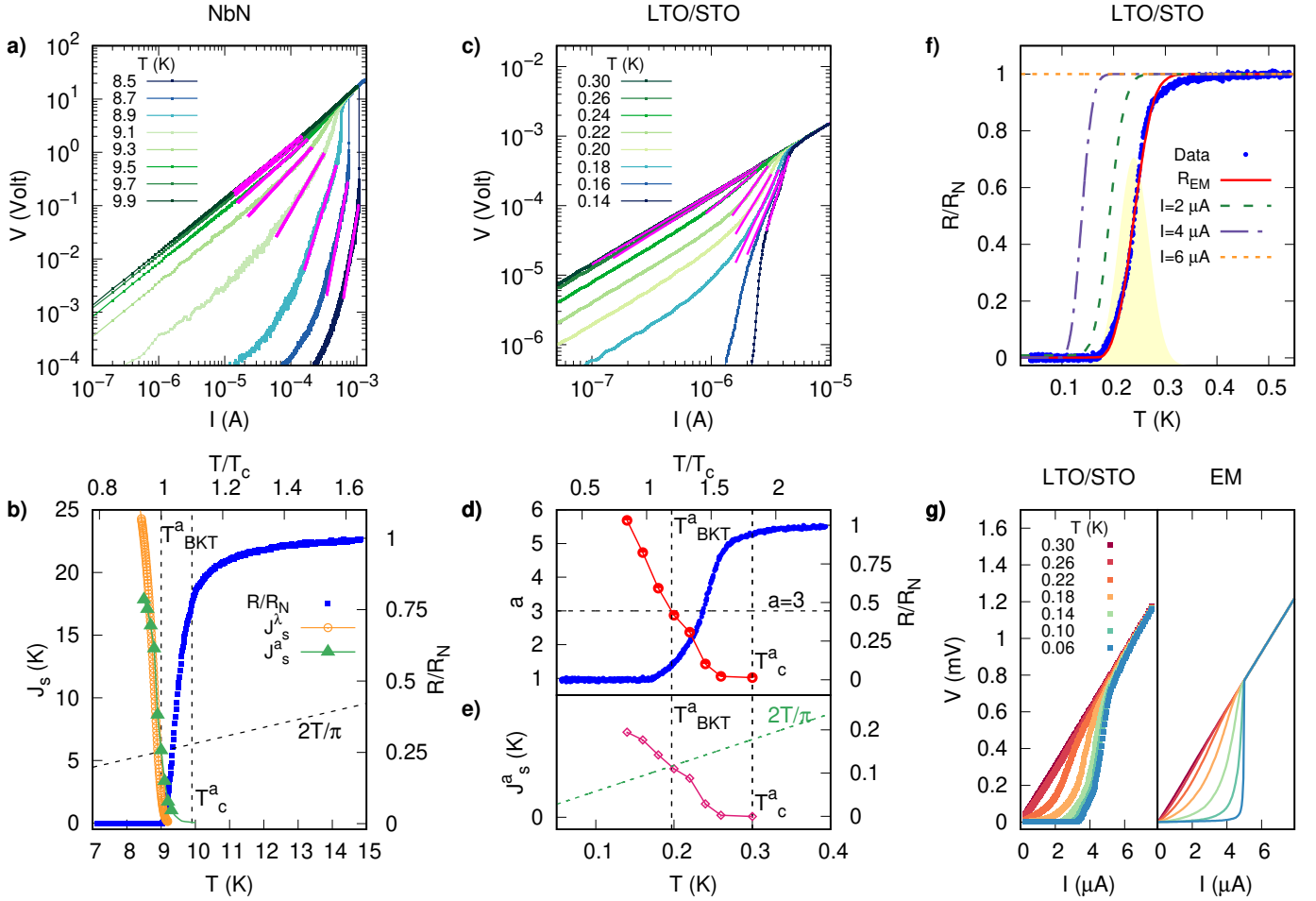


Figure 2. (a)-(b) Experimental results for a 3nm thick NbN film. (a) Measurements of the IV characteristics. Solid lines are fit with the Eq. (1). (b) Temperature dependence of the measured superfluid stiffness J_s^a , compared with the one extracted from IV characteristics, J_s^λ , and with the normalized resistivity (right axis). The universal $2T/\pi$ BKT line is also shown. The slightly larger value of the SC transition T_c^a extracted from J_s^a can be ascribed by finite-size effects. (c)-(d) Experimental results for a LTO/STO sample. (c) Measurements of the IV characteristics. Solid lines are fit with the Eq. (1). The resulting exponent $a(T)$ is shown in panel (d), along with the normalized sheet resistance. (e) Superfluid stiffness J_s^a extracted from the $a(T)$ exponent, along with the BKT critical line $2T/\pi$. (f)-(g) Comparison between the LTO/STO data and the theoretical results obtained within the EM approximation. (f) Normalised sheet resistance R/R_N (blue dots) compared with the EM resistivity R_{em} obtained from the numerical solution of Eq. (2) at $I = 0$ (solid red line) and at finite I (dashed lines). In background we show the probability distribution of T_c^i , with $\bar{T}_c = 0.24$ K and $\sigma = 0.029$ K. (g) Experimental (left) and theoretical (right) $V(I)$ curves at different temperatures. For the EM calculations we used a larger variance $\sigma = 0.06$ K and $I_{c,0} = 5$ μ A.

We now turn to the case of STO-based interfaces. Fig. 2c shows the IV characteristics of a LTO/STO sample. The first observation is the presence of a persistent non-linear behavior over a wide temperature range *above* T_c , which is identified by the vanishing of the dc resistivity. This has to be contrasted with the case of NbN, where at $T \simeq 1.1 T_c$ the IV characteristics display a full linear behavior, as indeed expected in the metallic case where vortices are already thermally unbound. While this simple observation should already suggest that at different mechanism is at play here, we can nonetheless pursue the BKT analysis based on Eq. (1), and extract the $a(T)$ exponent, see Fig. 2d. The corresponding $J_s^a(T)$, shown in Fig. 2e, vanishes at a temperature T_c^a *twice* as

large as the SC critical temperature T_c , and even the temperature T_{BKT}^a where J_s^a intersects the BKT line is above T_c , highlighting the failure of the BKT analysis. Notice that similar findings for the IV characteristics are very common in the literature in STO-based interfaces[46–48] and other gated 2D superconductors[3, 51–53].

To explain the IV non-linearity in LTO/STO we then propose a simple model, starting from the basic idea that in these systems transport is dominated by percolation through a strongly inhomogeneous background emerging at mesoscopic length scales[8, 39–42]. By closer inspection of Fig. 2c one sees that the non-linear regime connects smoothly to the linear one, while for NbN in Fig. 2a the non-linear regime is followed by an abrupt jump at

the critical current where normal-state resistance is recovered. Such a difference is due to the fact that in LTO/STO one is in practice analysing non-linear characteristics *above* T_c , where no SC critical current exists but the resistivity is strongly temperature dependent. As already observed before [7, 25, 45], such a broadening of the resistive SC transition cannot be ascribed to usual paraconductivity effects due to SC fluctuations. Instead, it can be well captured by assuming that the metal-to-superconductor transition can be mapped onto a random-resistor-network problem. We then consider a set of local resistances R_i which switch off from the normal-state value R_N to zero at a local temperature T_c^i , whenever the driving current I is below a threshold I_c^i . The local T_c^i are distributed with a probability $P(T_c^i)$, with overall weight $w_s = \int dT_c^i P(T_c^i)$. The SC transition can be well understood already in the EM approximation [7, 45], where the sample resistance $R_{em}(T, I)$ is a solution of the self-consistency equation [5, 6]

$$\sum_i \frac{R_i - R_{em}}{R_i + R_{em}} = 0, \quad (2)$$

where each R_i has a probability $w(T) = \int_T^\infty dT_c^i P(T_c^i)$ of being zero [49]. Even though the EM approach neglects spatial correlations, nonetheless it gives insight about the qualitative behaviour of the system. At $I = 0$ the condition $R_{em} = 0$ requires that the fraction $w(T)$ of SC links has reached the percolation threshold w^* (in two dimensions, $w^* = 0.5$, see [49] for more details). The shape of $R_{em}(T, I = 0)$ depends on the width of the $P(T_c^i)$ distribution, that sets the width of the paraconductivity regime, and on the total fraction w_s of SC links. When w_s is smaller than one, i.e., part of the system remains metallic, and slightly larger than the percolation threshold, i.e., $w_s \gtrsim 0.5$, one finds [7] that R_{em} has a marked tail above T_c , as shown by the numerical solution of Eq. (2) in Fig. 2f, in agreement with the experiments. Here, we assumed that the T_c^i distribution is gaussian, with average $\bar{T}_c = 0.24$ K and standard deviation $\sigma = 0.029$ K, and we used $w_s = 0.52$. As a consequence, when the temperature decreases below $\bar{T}_c + 3\sigma \simeq 0.29$ K the condition $T < T_c^i$ is fulfilled for a progressively larger fraction of local resistors R_i , which then switch off to zero, leading to a suppression of $R_{em}(T, I = 0)$.

A finite driving current is then able to break the weak links between the good SC regions having mesoscopic length scales. Even though we lack a precise information on the nature of the microscopic weak links, we checked [49] that the experimental data can be well reproduced by a temperature-dependent critical current following the Ambegaokar-Baratoff formula [9]:

$$I_c^i = I_{c,0} \frac{\Delta_i(T)}{\Delta_i(0)} \tanh \left(\frac{\Delta_i(T)}{2k_B T} \right) \quad (3)$$

where $I_{c,0}$ at $T = 0$ is independent of the resistor, and the $T = 0$ value of the local gap scales with the local T_c^i

as $\Delta_i(0)/k_B T_c^i \approx 1.76$. We notice that the temperature dependence of I_c following from Eq. (3) is also in good agreement with a recent analysis of the critical current at STO-based interfaces [8]. From Eq. (3) we see that, at a given temperature, only the resistors having I_c^i larger than the driving current I can be SC. This leads to a shift of the $R_{em}(T, I)$ curves towards lower temperatures, for increasing current, as shown in Fig. 2f. The same effect is also responsible for the observed non-linearity of the IV characteristics shown in Fig. 2g. Here we used $I_{c,0} = 5 \mu\text{A}$ and a somehow larger width $\sigma = 0.06$ K of the $P(T_c^i)$ distribution. Despite the simplifications implicit in our model, with this set of parameters we can very well reproduce the experimental curves. Below T_c all the I_c^i rapidly collapse towards $I_{c,0}$, which essentially identifies the real critical current in the SC state (see also [49] for further details). On the other hand, above T_c , in the whole regime of temperatures where $R_{em}(T, I = 0) \ll R_N$ because of the sample inhomogeneity, the non-linear behavior is due to the current-induced breaking of the SC links. As I increases a larger fraction of the SC link becomes normal, and the global resistivity progressively crosses over towards its normal-state value. Finally, the wider distribution of T_c^i found in the analysis of IV characteristics may be ascribed to the possible occurrence of avalanche effects that are not easily captured by our simple model. Indeed, as soon as the first weak link breaks down, more current is expected to go through the remaining SC links, which then will be easier to break and so on. As a consequence, the distribution of local SC links can get broader at larger applied currents, as indeed we found while comparing the theoretical simulation with the experiments.

In summary, we analyzed the IV characteristics in two paradigmatic examples of 2D superconductors: NbN thin films, and STO-based oxide interfaces. In the former case we observed a non-linear behavior that is well consistent with the BKT physics. Indeed, even if nanoscopic inhomogeneity of the SC background can partly hinder the manifestation of the BKT signatures, as the universal BKT jump, its essential features remain visible. In contrast, in STO-based interfaces the non-linear IV characteristics cannot be ascribed to a BKT phenomenon, rather to the existence of a strong fragmentation of the SC properties on mesoscopic length scales. By modelling the SC transition with a percolative model, where the fraction of SC regions depends both on the temperature and on the driving current, we can well reproduce the observed non-linearity of the transport. A behavior of the IV characteristics similar to the one observed in our LTO/STO sample is very common in the literature, especially for gated superconductors. Indeed, it has been seen in other STO-based interfaces [46–48], in 2D transition-metal dichalcogenides [51–53] and also in the recently discovered twisted bilayer graphene [3]. As a consequence, while our results question the possibility to observe a

BKT physics in this extremely confined 2D electron gas, they also suggest that non-linear IV characteristics can be used as a benchmark for emergent inhomogeneity in a wide class of superconductors.

Acknowledgements

The work was supported by talia-India collaborative project SuperTop (Italian MAECI PGRO4879 and Indian Department of Science and Technology No. INT/Italy/P-21/2016 (SP)), by the Sapienza University via Ateneo 2017 (prot. RM11715C642E8370) and Ateneo 2018 (prot. RM11816431DBA5AF), by the Department of Atomic Energy, Govt. of India, Department of Science and Technology, Govt. of India (Grant No: EMR/2015/000083), by the IFCPAR French-Indian program (Contract No. 4704-A), by the Delegation G n rale   l'Armement (which supported the PhD grant of SH), and by the Nano-SO2DEG project of the JCJC program of the ANR.

Authors contribution MM, JJ and PR synthesized the NbN sample and performed the measurements on it, AD and RCB provided the LTO/STO sample and JB, SH, NB and JL performed the measurements on it, GV, SC and LB elaborated the theoretical model and GV performed the numerical calculations. LB conceived the project together with SC, NB and PR. LB wrote the manuscript with inputs from all the coauthors.

* lara.benfatto@roma1.infn.it

- [1] Yu Saito, Tsutomu Nojima and Yoshihiro Iwasa, *Nature Rev. Mat.* **2**, 16094 (2016).
- [2] S. Gariglio, M. Gabay and J. M. Triscone, *APL Materials* **4**, 060701 (2016).
- [3] Yuan Cao, Valla Fatemi, Shiang Fang, Kenji Watanabe, Takashi Taniguchi, Efthimios Kaxiras and Pablo Jarillo-Herrero, *Nature* **556**, 43 (2018).
- [4] V. L. Berezinskii, *Sov. Phys. JETP* **34**, 610 (1972).
- [5] J. M. Kosterlitz and D. J. Thouless, *J. Phys. C* **6**, 1181 (1973).
- [6] J. M. Kosterlitz, *J. Phys. C* **7**, 1046 (1974).
- [7] M.R. Beasley, J.E. Mooij and T.P. Orlando, *Phys. Rev. Lett.* **2**, 1165 (1979).
- [8] D.R. Nelson and J.M. Kosterlitz, *Phys. Rev. Lett.* **39**, 1201 (1977).
- [9] B. I. Halperin and D. R. Nelson, *J. Low. Temp. Phys.* **36**, 599 (1979).
- [10] K. Epstein, A. M. Goldman, and A. M. Kadin, *Phys. Rev. Lett.* **47**, 534 (1981).
- [11] K. Epstein, A. M. Goldman, and A. M. Kadin, *Phys. Rev. B* **27**, 6691 (1983).
- [12] A. T. Fiory, A. F. Hebard, and W. I. Glaberson, *Phys. Rev. B* **28**, 5075 (1983).
- [13] S. J. Turneaure, T. R. Lemberger, and J. M. Graybeal, *Phys. Rev. Lett.* **84**, 987 (2000).
- [14] R.W. Crane, N. P. Armitage, A. Johansson, G. Sambandamurthy, D. Shahar, and G. Gruner, *Phys. Rev. B* **75**, 094506 (2007).
- [15] W. Liu, M. Kim, G. Sambandamurthy, and N.P. Armitage, *Phys. Rev. B* **84**, 024511 (2011).
- [16] A. Kamlapure, M. Mondal, M. Chand, A. Mishra, J. Jesudasan, V. Bagwe, L. Benfatto, V. Tripathi, and P. Raychaudhuri, *Appl. Phys. Lett.* **96**, 072509 (2010).
- [17] M. Mondal, S. Kumar, M. Chand, A. Kamlapure, G. Saraswat, G. Seibold, L. Benfatto, and P. Raychaudhuri, *Phys. Rev. Lett.* **107**, 217003 (2011).
- [18] S. Misra, L. Urban, M. Kim, G. Sambandamurthy, and A. Yazdani, *Phys. Rev. Lett.* **110**, 037002 (2013).
- [19] Jie Yong, T. Lemberger, L. Benfatto, K. Ilin, M. Siegel, *Phys. Rev. B* **87**, 184505 (2013).
- [20] Rini Ganguly, Dipanjan Chaudhuri, Pratap Raychaudhuri, Lara Benfatto, *Phys. Rev. B* **91**, 054514 (2015).
- [21] Julie A. Bert, Katja C. Nowack, Beena Kalisky, Hilary Noad, John R. Kirtley, Chris Bell, Hiroki K. Sato, Masayuki Hosoda, Yasayuki Hikita, Harold Y. Hwang, and Kathryn A. Moler, *Phys. Rev. B* **86**, 060503(R) (2012).
- [22] G. Singh, A. Jouan, L. Benfatto, F. Couedo, P. Kumar, A. Dogra, R. Budhani, S. Caprara, M. Grilli, E. Lesne, A. Barthelemy, M. Bibes, C. Feuillet-Palma, J. Lesueur, N. Bergeal, *Nat. Comm.* **9**, 407 (2018).
- [23] Nicola Manca, Daniel Bothner, Ana M. R. V. L. Monteiro, Dejan Davidovikj, Yildiz G. Saglam, Mark Jenkins, Marc Gabay, Gary Steele, and Andrea D. Caviglia, *Phys. Rev. Lett.* **122**, 036801 (2019).
- [24] G. M. Wysin, A. R. Pereira, I. A. Marques, S. A. Leonel, and P. Z. Coura, *Phys. Rev. B* **72**, 094418 (2005).
- [25] L. Benfatto, C. Castellani and T. Giamarchi, *Phys. Rev. B* **80**, 214506 (2009).
- [26] A. Erez and Y. Meir, *Europhys. Lett.* **91**, 47003 (2010).
- [27] L. Benfatto, C. Castellani and T. Giamarchi, *Berezinskii-Kosterlitz-Thouless Transition within the Sine-Gordon Approach: The Role of the Vortex-Core Energy*, invited chapter for *40 Years of Berezinskii-Kosterlitz-Thouless Theory*, edited by Jorge V. Jos  (World Scientific, Singapore, 2013).
- [28] E. J. Konig, A. Levchenko, I. V. Protopopov, I. V. Gornyi, I. S. Burmistrov, and A. D. Mirlin, *Phys. Rev. B* **92**, 214503 (2015).
- [29] A. Erez and Y. Meir, *Phys. Rev. Lett.* **111**, 187002 (2013).
- [30] I. Maccari, L. Benfatto, and C. Castellani, *Phys. Rev. B* **96**, 060508 (R) 2017
- [31] I. Maccari, L. Benfatto, and C. Castellani, *Condens. Matter* **3**(1), 8 (2018)
- [32] B. Sac p , C. Chapelier, T. I. Baturina, V. M. Vinokur, M. R. Baklanov, M. Sanquer, *Nature Communications* **1**, 140 (2010). B. Sac p  *et al.*, *Nature Phys.* **7**, 239 (2011).
- [33] M. Mondal, A. Kamlapure, M. Chand, G. Saraswat, S. Kumar, J. Jesudasan, L. Benfatto, V. Tripathi, and P. Raychaudhuri, *Phys. Rev. Lett.* **106**, 047001 (2011).
- [34] A. Kamlapure, T. Das, S. Chandra Ganguli, J. B. Parmar, S. Bhattacharyya, and P. Raychaudhuri, *Sci. Rep.* **3**, 2979 (2013).
- [35] Y. Noat, V. Cherkez, C. Brun, T. Cren, C. Carbillet, F. Debontridder, K. Ilin, M. Siegel, A. Semenov, H.-W. Hubers, D. Roditchev, *Phys. Rev. B* **88**, 014503 (2013).
- [36] C. Brun, T. Cren, V. Cherkez, F. Debontridder, S. Pons, D. Fokin, M. C. Tringides, S. Bozhko, L. B. Ioffe, B. L. Altshuler and D. Roditchev, *Nat. Phys.* **10**, 444 (2014).
- [37] C. Carbillet, S. Caprara, M. Grilli, C. Brun, T. Cren,

- F. Debontridder, B. Vignolle, W. Tabis, D. Demaille, L. Largeau, K. Ilin, M. Siegel, D. Roditchev, and B. Leridon, Phys. Rev. B **93**, 144509 (2016).
- [38] C. Brun, T. Cren and D. Roditchev, Supercond. Sci. Technol. **30**, 013003 (2017)
- [39] J. Biscaras, N. Bergeal, S. Hurand, C. Feuillet-Palma, A. Rastogi, R. C. Budhani, M. Grilli, S. Caprara, and J. Lesueur, Nat. Mater. **12**, 542 (2013).
- [40] Gopi Nath Daptary, Shelender Kumar, Pramod Kumar, Anjana Dogra, N. Mohanta, A. Taraphder, and Aveek Bid, Phys. Rev. B **94**, 085104 (2016).
- [41] G. E. D. K. Prawiroatmodjo, F. Trier, D. V. Christensen, Y. Chen, N. Pryds, and T. S. Jespersen Phys. Rev. B **93**, 184504 (2016).
- [42] N. Scopigno, D. Bucheli, S. Caprara, J. Biscaras, N. Bergeal, J. Lesueur, and M. Grilli, Phys. Rev. Lett. **116**, 026804 (2016).
- [43] S. Hurand, A. Jouan, E. Lesne, G. Singh, C. Feuillet-Palma, M. Bibes, A. Barthélémy, J. Lesueur, and N. Bergeal, Phys. Rev. B **99**, 104515 (2019).
- [44] S. Caprara, M. Grilli, L. Benfatto, C. Castellani, Phys. Rev. B **84**, 014514 (2011).
- [45] S. Caprara, D. Bucheli, N. Scopigno, N. Bergeal, J. Biscaras, S. Hurand, J. Lesueur and M. Grilli, Supercond. Sci. Technol. **28** 014002 (2015).
- [46] N. Reyren, S. Thiel, A. Caviglia, L. F. Kourkoutis, G. Hammerl, C. Richter, C. Schneider, T. Kopp, A.-S. Ruetschi, D. Jaccard, M. Gabay, D. Muller, J.-M. Triscone, and J. Mannhart, Science **317**, 1196 (2007).
- [47] Y.-L. Han, S.-C. Shen, J. You, H.-O. Li, Z.-Z. Luo, C.-J. Li, G.-L. Qu, C.-M. Xiong, R.-F. Dou, L. He, D. Naugle, G.-P. Guo, and J. Nie, Appl. Phys. Lett. **105**, 192603 (2014).
- [48] A. M. R. V. L. Monteiro, D. J. Groenendijk, I. Groen, J. de Bruijkere, R. Gaudenzi, H. S. J. van der Zant, and A. D. Caviglia, Phys. Rev. B **96**, 020504(R) (2017).
- [49] See Supplementary Material at...
- [50] Indranil Roy, Prashant Chauhan, Harkirat Singh, Sanjeev Kumar, John Jesudasan, Pradnya Parab, Rajdeep Sensarma, Sangita Bose, and Pratap Raychaudhuri, Phys. Rev. B **95**, 054513 (2017).
- [51] J. M. Lu, O. Zheliuk, I. Leermakers, N. F. Q. Yuan, U. Zeitler, K. T. Law, J. T. Ye, Science **350**, 1353 (2015)
- [52] L. J. Li, E. C. T. O'Farrell, K. P. Loh, G. Eda, B. Ozyilmaz, and A. H. Castro Neto, Nature **529**, 185 (2016).
- [53] A. W. Tsen, B. Hunt, Y. D. Kim, Z. J. Yuan, S. Jia, R. J. Cava, J. Hone, P. Kim, C. R. Dean and A. N. Pasupathy, Nature Physics **12**, 208 (2016).
- [54] R. Landauer, in *Electrical Transport and Optical Properties of Inhomogeneous Media*, edited by J. C. Garland and D. B. Tanner (American Institute of Physics, New York, 1978), p. 2.
- [55] S. Kirkpatrick, Rev. Mod. Phys. **45**, 574 (1973).
- [56] V. Ambegaokar and A. Baratoff, Phys. Rev. Lett. **10**, 486 (1962); erratum, **11**, 104 (1963).

Supplementary Material for Non-linear IV characteristics in two-dimensional superconductors: Berezinskii-Kosterlitz-Thouless physics vs inhomogeneity

EXPERIMENTAL DETAILS

NbN sample The measurement of $1/\lambda^2$ by means of two-coils mutual inductance were performed on a 3 nm thick NbN film grown on single crystalline MgO substrate. Details of sample preparation are given in [S1], and details of the two-coils technique can be found in [S1–S3]. As shown in Ref. [S1], the corresponding superfluid stiffness J_s^λ closely follows at low temperatures the BCS temperature dependence. However, as T_c is approached one observes a rapid deviation from the BCS fit. By accounting for a moderated inhomogeneity of the sample, and for the small vortex-core energy, one can indeed identify this downturn with the universal BKT jump, smeared by disorder[S1].

The IV measurements were performed by means of a standard 4-probe technique, by using a current source and a nanovoltmeter in a conventional ^4He cryostat where the sample is kept in contact with helium exchange gas to minimize heating effects. The temperature variation in all IV scans was less than 30 mK. To improve sensitivity, the film was patterned into a 20 μm wide stripline using ion-beam milling with large current contacts and narrow voltage contacts. In Fig. S1a we report the full data set of the IV characteristics, along with the fit done with Eq. (1) of the manuscript. The resulting $a(T)$ coefficient is shown in Fig. S1b, along with the resistivity curve

STO-based sample For what concerns the case of STO-based interfaces, in this experiment we used a 10 u.c thick LaTiO_3 epitaxial layer grown on a TiO_2 -terminated SrTiO_3 single by Pulsed Laser Deposition[S4]. The 3×3 mm LTO/STO sample was thermally anchored to the last stage of a dilution refrigerator and standard four probes resistivity measurements were performed in a Van der Pauw geometry.

THEORETICAL MODEL

The effective medium approximation for the random-resistor network

As explained in the main text, to simulate the mesoscopic inhomogeneity in STO-based samples we described the inhomogeneous SC background by means of a random resistor network (RRN) model. In this picture, every bond represents a resistor R_i , made by a mesoscopic region of electrons, with a specific local critical tempera-

ture T_c^i randomly distributed. The global resistance R_{em} of the system is given, within the effective-medium approximation (EMA), as a solution of the following self-consistent equation in two dimensions[S5, S6]:

$$\sum_i \frac{R_{em} - R_i}{R_{em} + R_i} = 0, \quad (\text{S1})$$

where the sum is carried over all the bonds. An equivalent way to rewrite Eq. (S1) is to sum instead over all possible values ρ attained by the local resistors, weighted with the corresponding probability distribution $p(\rho)$:

$$\int p(\rho) \frac{R_{em} - \rho}{R_{em} + \rho} = 0. \quad (\text{S2})$$

Suppose now that the each resistor can take only two constant values: $R_i = R_N$ if the link is in the normal-state, and $R_i = 0$ if the temperature is lowered below the bond critical temperature T_c^i , so the temperature dependence in each bond will be $R_i = R_N \theta(T - T_c^i)$, where $\theta(x)$ is the Heavyside step function. If we denote with $P(T_c^i)$ the probability distribution of the local critical temperatures, the probability distribution of resistivity in Eq. (S2) is then $p(\rho) = w(T)\delta(\rho) + [1 - w(T)]\delta(\rho - R_N)$, where $w(T) \equiv \int_T^{+\infty} P(T_c^i) dT_c^i$ is the statistical weight of the superconducting fraction. Eq. (S2) then reduces to:

$$w + (1 - w) \frac{R_{em} - R_N}{R_{em} + R_N} = 0. \quad (\text{S3})$$

The critical temperature T_c of the network, i.e. the temperature where $R_{em} \rightarrow 0$, is then defined by Eq. (S3) as the temperature where the SC fraction reaches the percolation threshold of $1/2$, as expected in two dimensions[S7]:

$$w(T_c) = \int_{T_c}^{+\infty} P(T_c) dT_c \equiv \frac{1}{2}. \quad (\text{S4})$$

For the distribution of local critical temperatures we assume a Gaussian distribution

$$P(T_c^i) = \frac{w_s}{\sqrt{2\pi}\sigma} e^{-\frac{(T_c^i - \bar{T}_c)^2}{2\sigma^2}} \quad (\text{S5})$$

with average value \bar{T}_c and variance σ , w_s representing the total fraction of SC regions in the material. To determine numerically the EMA solution we will resort to the form (S1), by randomly sampling the local T_c^i of each resistor according to the distribution (S5). At each temperature

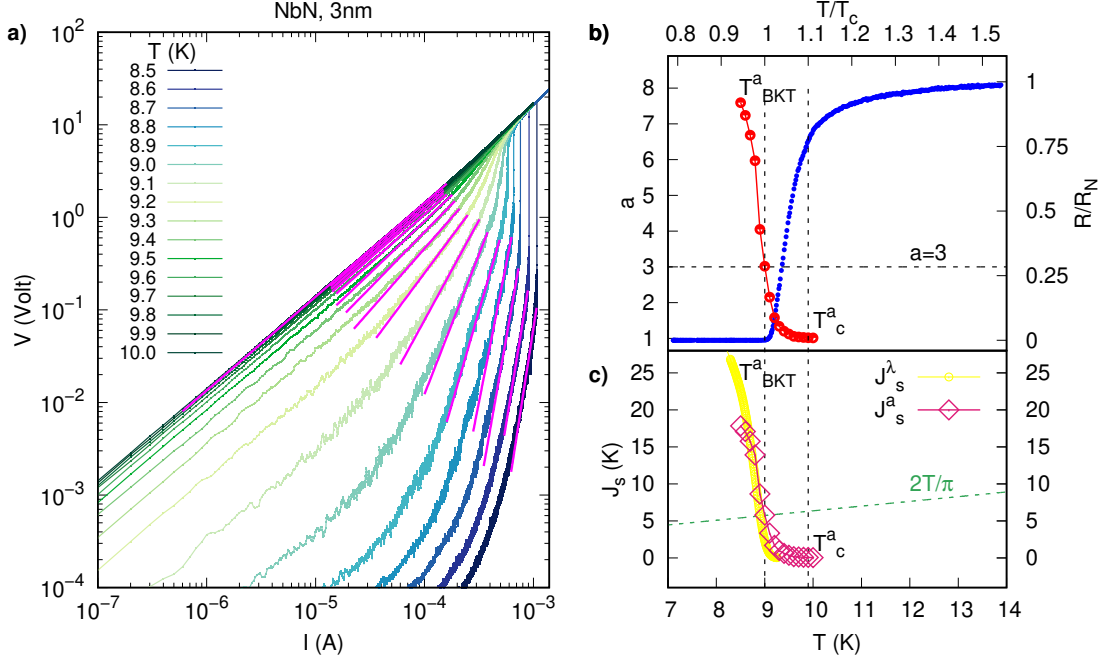


Figure S1. (a) Measurements of the IV characteristics for our 3nm NbN thin film. The same data at selected temperatures are shown in Fig. 2a of the main text. Solid lines are fit with the Eq. (1) of the main manuscript. (b) Temperature dependence of the corresponding $a(T)$ parameter, compared with the resistivity. (c) Temperature dependence of the superfluid stiffness J_s^a extracted from the $a(T)$ exponent, compared to the stiffness J_s^λ obtained by means of direct two-coils mutual inductance technique.

T a fraction $\int_T^\infty dT_c^i P(T_c^i)$ of bonds are "switched-off", following the condition

$$R_i = \begin{cases} 1, & \text{if } T_c^i < T \\ 0, & \text{if } T_c^i \geq T \end{cases} \quad (\text{S6})$$

so that the effective resistivity R_{em} will diminish by lowering the external temperature, until the percolation threshold $w = 0.5$ is reached and R_{em} becomes zero. This procedure is more convenient than the numerical solution of Eq. (S2) to implement the effects of a finite current, as we shall see in the next section.

Effects of a finite current

Starting from the EMA, the information about the local critical temperature of each bond can be easily implemented as:

$$R_i(T, I) = \begin{cases} 1, & \text{if } T \geq T_c^i, \\ 0, & \text{if } T < T_c^i, I \leq I_c^i, \\ 1, & \text{if } T < T_c^i, I > I_c^i, \end{cases} \quad (\text{S7})$$

where I_c^i is the critical current of the i -th bond. In the absence of a full microscopic model for the SC puddles, we analyzed different critical-current schemes for the relation $I_c^i = f(T_c^i, T)$ and compared them with the

data, in order to get an insight on the physical mechanism at play. The simplest relation one can guess is the Ginzburg-Landau (GL) relation for the critical current:

$$I_c^i = I_0^i(T)(T_c^i - T)^{3/2}. \quad (\text{S8})$$

Here $I_0^i(T)$ sets the magnitude of the current, depending on the microscopic structure of the material; in principle, it can be a function of the external temperature T and it can depend on the single resistor. As a starting point, we consider the easiest case $I_0^i(T) = I_0$ so the function is analytically invertible and therefore, for the i -th resistor to be superconducting, the condition to be fulfilled is $T_c^i \geq T + (I/I_0)^{2/3}$. We thus have

$$R_i = \begin{cases} 1, & \text{if } T_c^i < T_{eff}, \\ 0, & \text{if } T_c^i \geq T_{eff}, \end{cases} \quad (\text{S9})$$

where $T_{eff} = T + \left(\frac{I}{I_0}\right)^{2/3}$ is the effective temperature perceived by the resistors. In this situation the R_{em} depends on the applied current and the IV characteristics will be in general non-linear.

In Fig.S2 we show the resistivity curve and the IV characteristics at different T in the GL case. The effective resistivity R_{em} (solid red curve in fig. S2a) fits well the experimental data at vanishing driving current, using parameters $w = 0.5$, $\sigma = 0.029$ K, $\bar{T}_c = 0.24$ K. At finite current, using $I_0 = 80 \mu\text{A}$, we obtain the

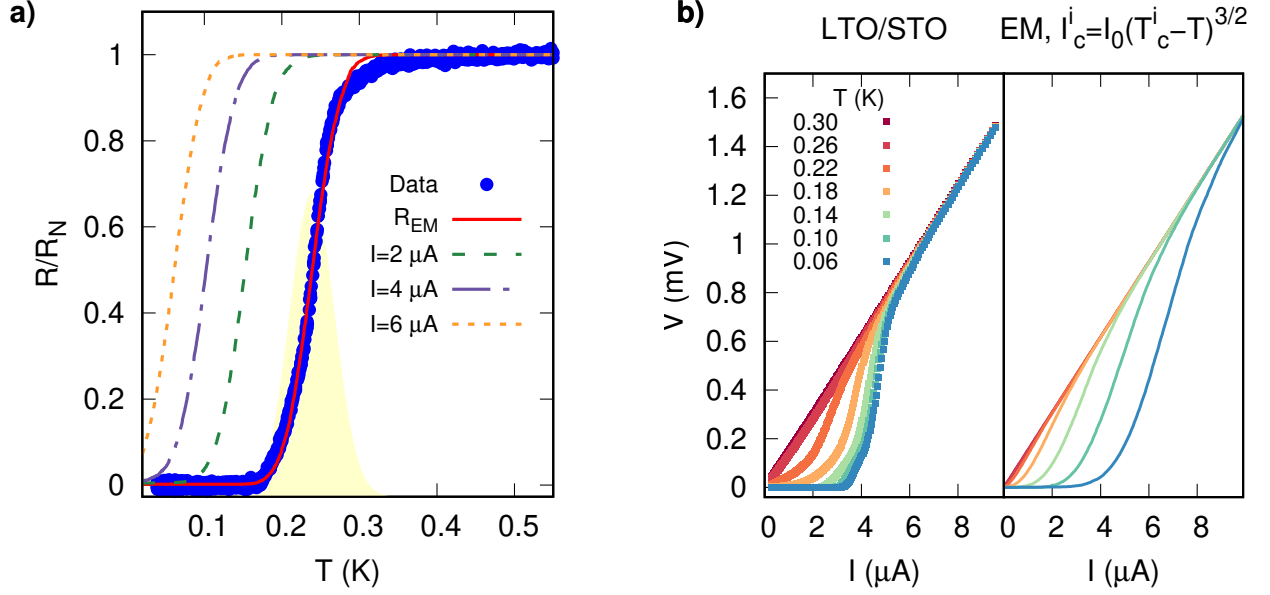


Figure S2. (a) Normalised sheet resistance R/R_N (blue dots) compared with the EM resistivity R_{em} obtained from the numerical solution of Eq. (S1) at $I = 0$ (solid red line) and at finite I (dashed lines). In background we show the probability distribution of T_c^i , with $w = 0.5$, $\bar{T}_c = 0.24$ K and $\sigma = 0.029$ K. (b) Experimental (left) and theoretical (right) $V(I)$ curves at different temperatures using the GL relation (S8).

$R_{em}(T, I)$ displayed in Fig. S2a with dashed lines. Despite the fact that one obtains in general an increasing of R_{em} as I increases for a fixed temperature, the agreement with the experimental IV curves is very poor. In fig. S2b we compare the experimental IV characteristics of our LTO/STO sample with the EMA numerical calculations. The experimental data display a tendency to recover the ideal behaviour of a homogeneous superconductor as the temperature decreases, i.e. $V \propto I(I - I_c)$ when $T \rightarrow 0^+$. This trend is not captured by the numerical calculation presented in the right panel of fig. S2b, which provide very broad IV characteristics, even at temperatures much lower than the percolation temperature $T_{perc} \simeq 0.19$ K. To understand the origin of such drawback, we computed the probability distribution $P_I(I_c)$ of the critical currents, that is directly related to $P(T_c^i)$ by $P_I(I_c) = \int \delta(I_c - f(T_c^i))P(T_c^i)dT_c^i$, where $I_c = f(T_c)$ is the functional relation between the local critical current and the local critical temperature. Given its inverse function $T_c = g(I_c)$ one simply gets

$$P_I(I_c) = \frac{P(g(I_c))}{|f'(g(I_c))|}. \quad (\text{S10})$$

where $P(x)$ is the distribution given in Eq. (S5).

For the GL model of the critical current we showed above that $f(T_c) = I_0(T_c - T)^{3/2}$ and $g(I_c) = T_{eff}$, so that $P_I(I_c)$ takes the following form:

$$P_I(I_c) = \frac{2w}{3\sigma\sqrt{2\pi}I_0^{2/3}} \frac{e^{-\frac{(I_c/I_0)^{4/3}}{2\sigma^2}}}{I_c^{1/3}}. \quad (\text{S11})$$

The main result is that in this case $P_I(I_c)$ does *not* depend on the external temperature T . This is also evident looking at the resistivity at finite I in fig. S2a, where all curves are obtained by shifting of the resistivity at $I = 0$. This is a consequence of the fact that in the GL case the effect of the finite current is just to redefine the effective temperature of the system, as given by Eq. (S9). In contrast, the experimental data shown in the left panel of fig. S2b suggest that while above T_c the system recovers smoothly the normal-state resistivity as I increases, i.e. a wide distribution of local I_c^i is present, as T decreases the V jumps almost suddenly to the normal-state value as I increasing, signalling that the distribution of local I_c values should progressively shrink towards a critical value $I_{c,0}$ that is the same for all the mesoscopic resistors.

These observations suggest that a different modelling for $I_c^i(T)$, able to satisfy two requirements: (i) the zero temperature critical current must be independent on the single resistor $I_{c,0}^i = \text{const}$, (ii) the critical current should saturate pretty fast to its zero-temperature value in order to recover the behaviour of IV curves at low temperature. The second item is also suggested by recent measurements in an other STO-based sample of the critical-current distribution below T_c [S8]. We then explored the outcomes of the Ambegaokar and Baratoff [S9] formulas, describing the critical current for a weak link between two SC electrodes

$$I_c R_N = \frac{\pi \Delta(T)}{2e} \tanh\left(\frac{\Delta(T)}{2k_B T}\right). \quad (\text{S12})$$

According to Eq. (S12) the critical current through a

constriction scales with the superfluid density, that is expected to follow a BCS-like relation with $J_S(T) = J_S(0) \frac{\Delta(T)}{\Delta(0)} \tanh\left(\frac{\Delta(T)}{2k_B T}\right)$. To mimic the BCS temperature dependence of the gap $\Delta_i(T)$ in each resistor we use a simple approximated formula that reproduces well the BCS behavior (see inset of Fig. S3a):

$$f(\tau^i) = \frac{\Delta_i(T)}{\Delta_i(0)} = \left(1 - \frac{\tau^4}{3}\right) \sqrt{1 - \tau^4}, \quad \frac{\Delta_i(0)}{k_B T_c^i} \simeq 1.76 \quad (\text{S13})$$

where $\tau^i = T/T_c^i$. The resulting temperature dependence of $I_c(T)$ from Eq. (S12) is shown in Fig. S3a. As mentioned above, the experimental data suggest that all resistors have the same critical current as $T \rightarrow 0$. We then assume for each local resistor the following temperature-dependent critical current:

$$I_c^i(T) = I_{c,0} f(\tau^i) \tanh\left(\frac{1.76}{2} \frac{f(\tau^i)}{\tau^i}\right), \quad (\text{S14})$$

so that all the local link have the same $I_{c,0}$ as $T \rightarrow T_c$ but their behavior is different as T approaches the local transition temperature T_c^i . The IV characteristics obtained from the model (S14) are shown in Fig. 2g of the main manuscript. As one can see, they reproduce very well the experimental findings. In particular, the model (S14) accounts for the sharpening of the RRN critical current as T is lowered below T_c , as one can see in Fig. S3b where we show the $P_I(I_c)$ obtained by inverting numerically the

T_c^i vs I_c^i relation from Eq. (S14). Here one recovers a narrowing of the critical-current distribution as T is lowered below $T_c \simeq 0.19$ K, and already for $T \simeq 0.06$ K $P_I(I_c)$ tends to a delta function centered at $I_{c,0}$.

* lara.benfatto@roma1.infn.it

- [S1] M. Mondal, S. Kumar, M. Chand, A. Kamlapure, G. Saraswat, G. Seibold, L. Benfatto, and P. Raychaudhuri, Phys. Rev. Lett. **107**, 217003 (2011).
- [S2] A. Kamlapure, M. Mondal, M. Chand, A. Mishra, J. Jesudasan, V. Bagwe, L. Benfatto, V. Tripathi, and P. Raychaudhuri, Appl. Phys. Lett. **96**, 072509 (2010).
- [S3] Indranil Roy, Prashant Chauhan, Harkirat Singh, Sanjeev Kumar, John Jesudasan, Pradnya Parab, Rajdeep Sensarma, Sangita Bose, and Pratap Raychaudhuri, Phys. Rev. B **95**, 054513 (2017).
- [S4] J. Biscaras, N. Bergeal, A. Kushwaha, T. Wolf, A. Rastogi, R.C. Budhani and J. Lesueur, Nat. Comm. **1**, 89 (2010)
- [S5] R. Landauer, in *Electrical Transport and Optical Properties of Inhomogeneous Media*, edited by J. C. Garland and D. B. Tanner (American Institute of Physics, New York, 1978), p. 2.
- [S6] S. Kirkpatrick, Rev. Mod. Phys. **45**, 574 (1973).
- [S7] S. Caprara, M. Grilli, L. Benfatto, C. Castellani, Phys. Rev. B **84**, 014514 (2011).
- [S8] S. Hurand, A. Jouan, E. Lesne, G. Singh, C. Feuillet-Palma, M. Bibes, A. Barthél  my, J. Lesueur, and N. Bergeal, Phys. Rev. B **99**, 104515 (2019).
- [S9] V. Ambegaokar and A. Baratoff, Phys. Rev. Lett. **10**, 486 (1962); erratum, **11**, 104 (1963).

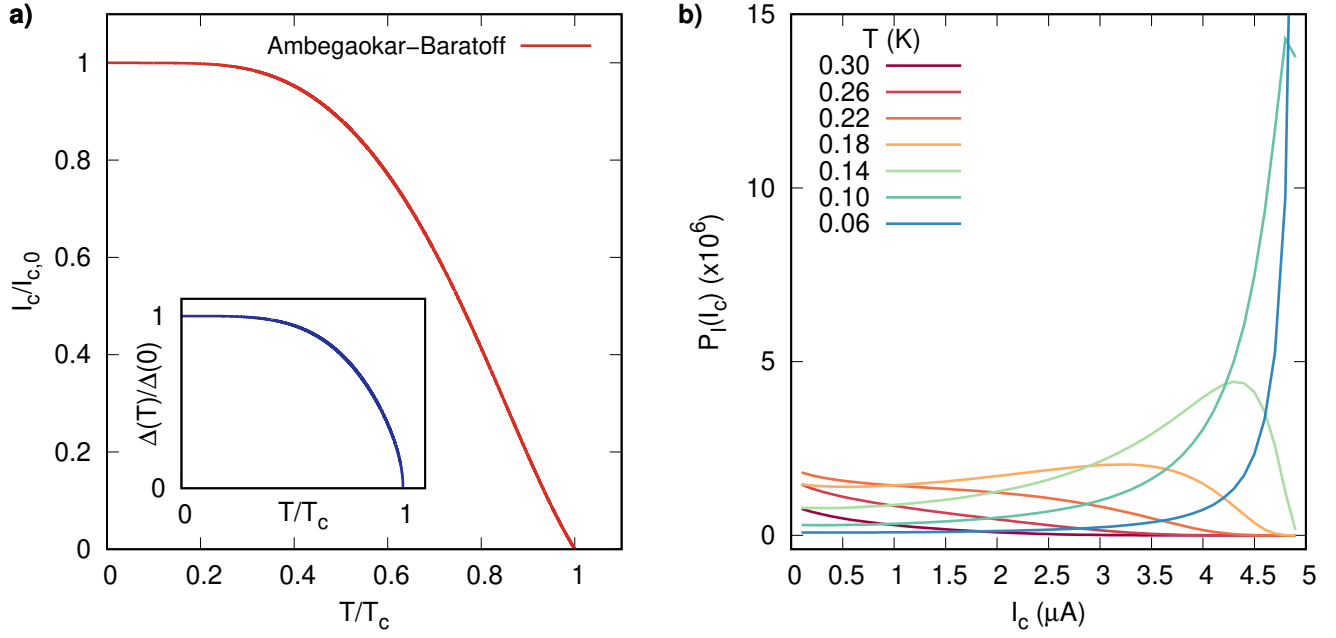


Figure S3. a) Temperature dependence of the critical current according to the Ambegaokar-Baratoff model (S14). Inset: approximated expression for the BCS-like temperature dependence of the gap, as given by Eq. (S13). (b) Probability distribution of the critical current for Ambegaokar-Baratoff model (S14), computed from Eq. (S10). The critical temperatures are distributed with the non-normalised Gaussian in Eq. (S5), using the fitting parameters $w = 0.52$, $\bar{T}_c = 0.24$ K, $\sigma = 0.06$ K and $I_{c,0} = 5 \mu A$